

## Recent Advances in III-Nitride Ultraviolet Photonic Materials and Devices

J. Y. LIN and H. X. JIANG\*

*Department of Physics, Kansas State University, Manhattan, KS 66506-2601, U.S.A.*

This paper summarizes some of the recent advances made on III-nitride ultraviolet photonics materials and devices. In particular, the growth and characterization of AlGa<sub>x</sub>N alloys are discussed in detail. It was shown that AlGa<sub>x</sub>N could be made n-type for  $x$  up to 1 (pure AlN). Time-resolved photoluminescence (PL) studies carried out on these materials have shown that Si-doping reduces the effect of carrier localization in Al<sub>x</sub>Ga<sub>1-x</sub>N alloys and a sharp drop in carrier localization energy occurs when the Si doping concentration increases above  $1 \times 10^{18} \text{ cm}^{-3}$ , which directly correlates with the observed electrical properties. For the Mg-doped Al<sub>x</sub>Ga<sub>1-x</sub>N alloys, p-type conduction was achieved for  $x$  up to 0.27. From the Mg acceptor activation energy as a function of Al content, the resistivity of Mg-doped Al<sub>x</sub>Ga<sub>1-x</sub>N with high Al contents can be estimated. For example, the projected resistivity of Al<sub>x</sub>Ga<sub>1-x</sub>N ( $x=0.45$ ) is around  $2.2 \times 10^4 \Omega\text{-cm}$ . Thus alternative methods for acceptor activation in AlGa<sub>x</sub>N or InAlGa<sub>x</sub>N with high Al contents must be developed before the high performance deep UV emitters can be realized.

PACS numbers: 78.47.+p, 78.55.Cr, 78.66.Fd

Keywords: Al<sub>x</sub>Ga<sub>1-x</sub>N, Wide bandgap, Time-resolved PL, Optical transitions, UV light emitters

### I. INTRODUCTION

There is currently a great need of solid-state ultraviolet (UV) emitters for the detection of chemical and biological agents as well as for the next-generation general lighting. In such applications based on III-nitride wide bandgap semiconductors, UV emitters with wavelengths shorter than 300 nm are needed and hence conductive n-type and p-type AlGa<sub>x</sub>N alloys with high Al contents are indispensable for carrier injection. For example, protein/bio-agent fluorescence is generally excited at 280 nm or 340 nm [1]. In a current bio-fluorescence detection system, a quadrupled Yttrium-Aluminum-Garnet (YAG) laser is used as the excitation source and photomultiplier tubes are used to detect the resulting fluorescence signals. The system is thus bulky and fragile. Furthermore, chip-scale detection (or micro-scale sensing) is not possible with current technology, which limit its use in many key applications. On the other hand, the current approach for generating white light is by coating the III-nitride blue LED chips with yellow or green phosphor [2-6]. This approach however suffers from severe color rendering and low power conversion efficiency problems. These problems can be greatly minimized by employing UV LEDs together with three-color phosphors for wavelength down conversion.

Although many of the ideas and potentials of III-nitride devices for UV applications have been identified, a transition from basic research to practical device components has not yet been made due to various technolog-

ical obstacles. For example, so far blue emitters based on III-nitrides exploit InGa<sub>x</sub>N/GaN QWs as active media [7]. In order to achieve UV emitters, quantum wells (QWs) based on the AlGa<sub>x</sub>N or InAlGa<sub>x</sub>N alloy system must replace the InGa<sub>x</sub>N/GaN QW active region. Additionally, the underneath n-GaN and the top p-GaN epilayers in blue emitters must also be replaced correspondingly by higher bandgap n- and p-type AlGa<sub>x</sub>N (or InAlGa<sub>x</sub>N) epilayers in order to provide carrier injection as well as minimize UV photon absorption.

Currently, achieving highly conductive AlGa<sub>x</sub>N and InAlGa<sub>x</sub>N alloys, especially p-type conductivity, with high Al contents remains one of the foremost challenging tasks of the Nitride community. Highly conductive AlGa<sub>x</sub>N alloys with Al contents ( $x$ ) as high as 0.6 - 0.7 are needed in 280 nm UV emitters. AlGa<sub>x</sub>N alloys with high Al contents, covering from 350 nm to 200 nm, cannot be replaced by any other semiconductor system due to the fact that no other semiconductors possess such a large direct bandgap (diamond is 5.4 eV with indirect bandgap).

Both n-type and p-type Al<sub>x</sub>Ga<sub>1-x</sub>N alloys with high  $x$  are very difficult to grow and to characterize due to their wide energy band gaps. In particular, high p-type conductivity in Al<sub>x</sub>Ga<sub>1-x</sub>N alloys is difficult to achieve due to the deepening of the Mg acceptor activation energy as well as reduced crystalline quality of the AlGa<sub>x</sub>N alloys with increasing Al content. Recently, highly conductive n-type Al<sub>x</sub>Ga<sub>1-x</sub>N epilayers for  $x$  up to 0.4 has been achieved by employing In-Si co-doping approach [8]. A few studies have been reported on Mg-doped p-type Al<sub>x</sub>Ga<sub>1-x</sub>N with low Al content ( $x \leq 0.15$ ) [9-12]. It was found that the activation energies ( $E_A$ ) of Mg acceptors

\*E-mail: jiang@phys.ksu.edu

Table 1. Electrical data of Si-doped  $\text{Al}_x\text{Ga}_{1-x}\text{N}$ . [after Ref. 13], Conduction ( $\Omega\cdot\text{cm}$ )<sup>-1</sup>, Mobility ( $\text{cm}^2/\text{Vs}$ )/concentration( $\text{cm}^{-3}$ ).

$N_{\text{Si}}(\text{cm}^{-3})\backslash x$	0.3	0.35	0.4	0.45	0.5
0	7.32 12/3.81 $\times 10^{18}$	0.47 23/1.29 $\times 10^{17}$	$5.2 \times 10^{-3}$ 8.6/3.81 $\times 10^{15}$	$2.6 \times 10^{-3}$ 3.1/5.30 $\times 10^{15}$	High resistivity
$5.0 \times 10^{17}$	0.4 9.6/2.60 $\times 10^{17}$	0.49 11/2.80 $\times 10^{17}$	0.16 4.8/2.11 $\times 10^{17}$	0.21 4.9/2.3 $\times 10^{17}$	0.23 5.2/2.81 $\times 10^{17}$
$1.0 \times 10^{18}$	0.62 13/2.99 $\times 10^{17}$	4.5 36/7.82 $\times 10^{17}$	0.67 10/4.17 $\times 10^{17}$	0.13 4.2/1.92 $\times 10^{17}$	0.013 3.1/2.66 $\times 10^{16}$
$2.5 \times 10^{18}$	15.3 61/1.57 $\times 10^{18}$	21.0 56/2.35 $\times 10^{18}$	15.4 60/1.60 $\times 10^{18}$	4.85 37/8.19 $\times 10^{17}$	<b>2.51</b> <b>16/9.82 <math>\times 10^{17}</math></b>
$5.0 \times 10^{18}$	25.7 45/3.57 $\times 10^{18}$	34.2 62/3.45 $\times 10^{18}$	10.0 19/3.16 $\times 10^{18}$	<b>10.2</b> <b>28/2.28 <math>\times 10^{18}</math></b>	0.88 14/3.94 $\times 10^{17}$

in Mg-doped  $\text{Al}_x\text{Ga}_{1-x}\text{N}$  increased with increase in Al content. Because these materials are of great importance in realizing nitride-based optoelectronic devices, studies that could provide better understanding and realization of highly conductive n-type and p-type  $\text{Al}_x\text{Ga}_{1-x}\text{N}$  alloys with high  $x$  ( $x \geq 0.4$ ) are urgently needed.

Here, we summarize recent results on the growth and characterization of  $\text{Al}_x\text{Ga}_{1-x}\text{N}$  alloys with  $x$  all the way up to 1.0. We have achieved highly conductive n-type  $\text{Al}_x\text{Ga}_{1-x}\text{N}$  alloys for  $x$  up to 0.7. A conductivity (resistivity) value of  $6.7 \Omega^{-1} \text{cm}^{-1}$  ( $0.15 \Omega\text{cm}$ ) [with free electron concentration  $2.1 \times 10^{18} \text{cm}^{-3}$  and mobility of  $20 \text{cm}^2/\text{Vs}$  at room temperature] has been achieved for  $\text{Al}_{0.65}\text{Ga}_{0.35}\text{N}$ , as confirmed by Hall-effect measurements [13]. Our experimental results also revealed that (i) the conductivity of  $\text{Al}_x\text{Ga}_{1-x}\text{N}$  alloys continuously increases with an increase of Si doping level for a fixed value of Al content and (ii) there exists a critical Si-dopant concentration of about  $1 \times 10^{18} \text{cm}^{-3}$  that is needed to convert insulating  $\text{Al}_x\text{Ga}_{1-x}\text{N}$  with high Al contents ( $x \geq 0.4$ ) to n-type. For the Mg-doped  $\text{Al}_x\text{Ga}_{1-x}\text{N}$  alloys, p-type conduction was achieved for  $x$  up to 0.27 [14]. The Mg acceptor activation energies  $E_A$  were obtained and found to increase almost linearly with Al content. We have also achieved for the first time the growth of high quality AlN epilayers that emit band-edge photoluminescence emission.

## II. EXPERIMENT

Si-doped  $\text{Al}_x\text{Ga}_{1-x}\text{N}$  alloys ( $1 \mu\text{m}$  thick) were grown on sapphire (0001) substrates with AlN buffer layers by MOCVD. The growth temperature and pressure were around  $1050 \text{ }^\circ\text{C}$  and 50 Torr, respectively. The metal organic sources used were trimethylgallium (TMGa) for Ga and trimethylaluminum (TMAI) for Al. The gas source used were blue ammonia ( $\text{NH}_3$ ) for N and Silane ( $\text{SiH}_4$ ) for Si doping and the doping level was varied

by controlling the  $\text{SiH}_4$  flow rate. The Al contents of Si-doped n-type  $\text{Al}_x\text{Ga}_{1-x}\text{N}$  alloys were determined by energy dispersive x-ray (EDX) microanalysis and x-ray diffraction (XRD) measurement as well as by the flow rates of TMGa and TMAI. The Al contents ( $x$ ) determined by all three methods agreed within  $\pm 0.02$ . The Si-dopant concentrations were determined by the flow rate of  $\text{SiH}_4$  as well as by the variable temperature Hall effect measurement at elevated temperatures ( $T < 650 \text{ K}$ ). Additionally, secondary ion mass spectroscopy (SIMS) measurements were performed (by Charles and Evan) for selective samples to verify the Si-dopant concentrations. Atomic force microscopy (AFM) and scanning electron microscopy (SEM) were employed to examine the surfaces and revealed crack-free  $\text{Al}_x\text{Ga}_{1-x}\text{N}$  epilayers. Variable temperature Hall-effect (Standard Van der Pauw) measurements were employed to measure the electron concentration, mobility, and resistivity of these materials.

A deep UV (10 mW @ 195 nm) picosecond time-resolved photoluminescence (PL) spectroscopy system was specially designed to probe the optical properties of materials and devices structures based on  $\text{Al}_x\text{Ga}_{1-x}\text{N}$  alloys with high  $x$  and hence serves as “eyes” for monitoring the material qualities of these materials. The picosecond time-resolved PL spectroscopy system basically consists of a frequency quadrupled 100 femtosecond Ti: sapphire laser with a 76 MHz repetition rate, a monochromator (1.3 m), and a streak camera with a detection capability ranging from 185 - 800 nm and a time resolution of 2 ps [15].

## III. RESULTS AND DISCUSSIONS

### 1. High Al-content n-type AlGa<sub>N</sub> alloys

Table 1 summarizes the results from the room temperature Hall-effect measurement of the 25  $\text{Al}_x\text{Ga}_{1-x}\text{N}$

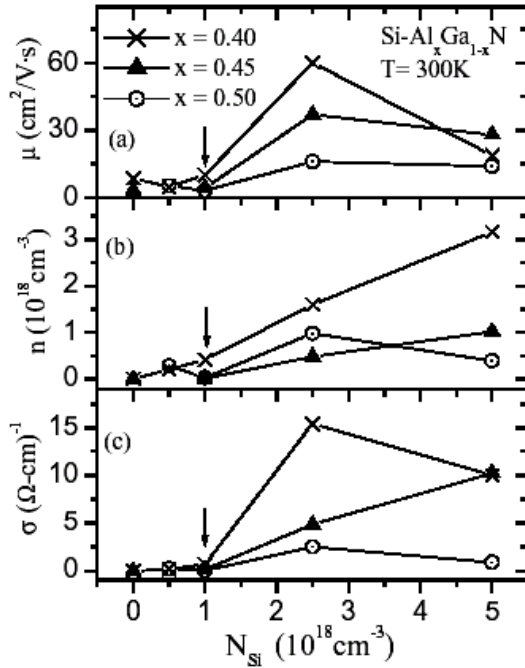


Fig. 1. (a) Mobility  $\mu$ , (b) electron concentration  $n$  and (c) conductivity  $\sigma$  of Si-doped  $\text{Al}_x\text{Ga}_{1-x}\text{N}$  alloys as a function of Si doping concentration  $N_{\text{Si}}$  for three different Al compositions  $x = 0.4, 0.45$  and  $0.5$  [after Ref. 13].

samples with  $x$  varying from 0.3 to 0.5 and the effective Si dopant concentration varying from 0 to  $5.0 \times 10^{18} \text{cm}^{-3}$ . The general trends are that the conductivity of  $\text{Al}_x\text{Ga}_{1-x}\text{N}$  alloys increases with the Si doping level,  $N_{\text{Si}}$  (for a fixed value of  $x$ ) and decreases with  $x$  (at a fixed value of  $N_{\text{Si}}$ ). Free electron concentrations as high as  $2.3 \times 10^{18} \text{cm}^{-3}$  (with a mobility of  $28 \text{cm}^2/\text{Vs}$ ) and  $1 \times 10^{18} \text{cm}^{-3}$  (with a mobility of  $16 \text{cm}^2/\text{Vs}$ ) have been achieved in  $\text{Al}_{0.45}\text{Ga}_{0.55}\text{N}$  and  $\text{Al}_{0.5}\text{Ga}_{0.5}\text{N}$  alloys, respectively. The data shown in Table 1 are plotted in Fig. 1 for representative samples (of  $x = 0.4, 0.45$ , and  $0.5$ ), showing variation of electron mobility, electron concentration, and conductivity of Si-doped  $\text{Al}_x\text{Ga}_{1-x}\text{N}$  alloys with Si doping concentrations  $N_{\text{Si}}$ . We see that the electron concentration, mobility, and conductivity all increase with increasing  $N_{\text{Si}}$ . In particular, Fig. 1 reveals that there exists a critical Si-doping concentration of about  $1 \times 10^{18} \text{cm}^{-3}$  for converting insulating  $\text{Al}_x\text{Ga}_{1-x}\text{N}$  with high Al contents ( $x \geq 0.4$ ) to n-type conductivity. We believe that this is a direct consequence of electrons filling the localized states in  $\text{Al}_{0.5}\text{Ga}_{0.5}\text{N}$  alloys caused by alloy fluctuation. Our results here suggest that below the mobility edge (energy that separates the localized states from the extended states), the density of the localized states in  $\text{Al}_x\text{Ga}_{1-x}\text{N}$  alloys with  $x \geq 0.4$  is on the order of  $1 \times 10^{18} \text{cm}^{-3}$ .

Fig. 2 shows room-temperature (300 K) PL spectra of  $\text{Al}_x\text{Ga}_{1-x}\text{N}$  with three different Si doping concentrations ( $N_{\text{Si}}$ ) at fixed Al content  $x = 0.4, 0.45$ , and  $0.5$ . In

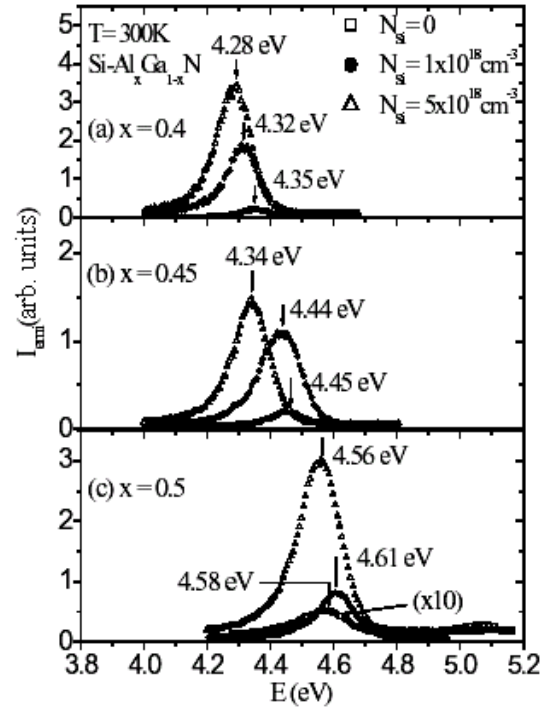


Fig. 2. Room temperature PL spectra of Si-doped  $\text{Al}_x\text{Ga}_{1-x}\text{N}$  alloys with three different doping concentrations for (a)  $x = 0.4$ , (b)  $x = 0.45$  and (c)  $x = 0.5$  [after Ref. 13].

addition to the shift of the peak positions ( $E_p$ ) toward longer wavelengths at higher doping levels due to the effect of the bandgap renormalization, we also observe a considerable increase in the PL emission intensity with increasing  $N_{\text{Si}}$ . The improvement of optical quality by Si doping has been observed previously in GaN epilayers [16–18] and AlGaIn/GaN multiple quantum wells [19]. The relative PL intensities for Si-doped  $\text{Al}_x\text{Ga}_{1-x}\text{N}$  alloys seen here increase by about one order of magnitude when the Si doping concentration is varied from 0 to  $5 \times 10^{18} \text{cm}^{-3}$ . For example, for  $x = 0.45$ , the relative PL emission intensity increases from 5 to 37 and to 44 as the doping concentration increases from 0 to  $1 \times 10^{18} \text{cm}^{-3}$  and to  $5 \times 10^{18} \text{cm}^{-3}$ .

To investigate the influence of the Si doping concentration on the carrier localization properties of the  $\text{Al}_x\text{Ga}_{1-x}\text{N}$  alloys, we measured the carrier localization energy and recombination lifetime as functions of Si doping for representative samples. Fig. 3 shows the Arrhenius plots of PL intensity for n-type  $\text{Al}_{0.45}\text{Ga}_{0.55}\text{N}$  epilayers with different Si doping levels up to  $5 \times 10^{18} \text{cm}^{-3}$ . The solid lines in Fig. 3 are the least squares fit of data with equation

$$I_{\text{emi}}(T) = I_0/[1 + C \exp(-E_0/kT)], \quad (1)$$

where  $E_0$  is the activation energy of the PL emission, which is a measure of the carrier localization energy. The fitted activation energies  $E_0$  are also indicated in Fig. 3. Time-resolved PL was employed to measure the

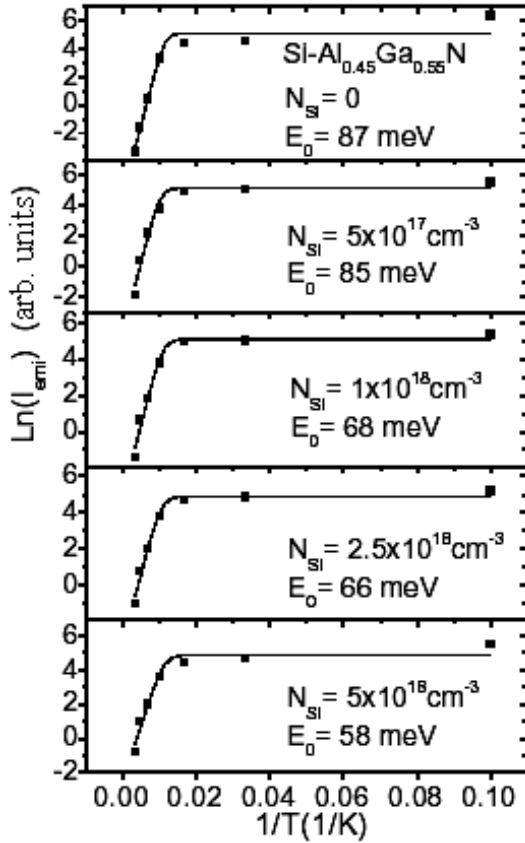


Fig. 3. The Arrhenius plots of integrated PL intensity for Si-doped  $\text{Al}_{0.45}\text{Ga}_{0.55}\text{N}$  alloys with different Si doping concentration  $N_{\text{Si}}$  ranging from 0 to  $5 \times 10^{18} \text{ cm}^{-3}$ . The solid lines are the least square fit of the data with Eq. (1) [after Ref. 13].

carrier recombination lifetimes at different doping levels. Fig. 4(a) shows temporal responses of PL emission of Si doped  $\text{Al}_{0.45}\text{Ga}_{0.55}\text{N}$  samples with three different doping concentrations measured at their respective spectral peak positions. It clearly shows a systematic decrease of the recombination lifetime with increasing  $N_{\text{Si}}$ . The recombination lifetime  $\tau$  and activation energy  $E_0$  of PL emission for Si-doped  $\text{Al}_{0.45}\text{Ga}_{0.55}\text{N}$  epilayers as functions of doping level are plotted in Fig. 4(b). Both values of  $\tau$  and  $E_0$  exhibit initial sharp decreases when the Si doping concentration is increased from  $N_{\text{Si}} = 0$  to  $N_{\text{Si}} = 1 \times 10^{18} \text{ cm}^{-3}$ , followed by gradual decreases as  $N_{\text{Si}}$  is further increased. These results suggest that Si-doping reduces the carrier localization effect with a sharp reduction in carrier localization energy taking place at around  $N_{\text{Si}} = 1 \times 10^{18} \text{ cm}^{-3}$ . The results shown in Fig. 4(b) thus corroborate the electrical data presented in Table 1 and in Fig. 1. Our results suggest that the critical Si-doping concentration needed to fill up the localized states in  $\text{Al}_x\text{Ga}_{1-x}\text{N}$  alloys ( $x \geq 0.4$ ) is around  $N_{\text{Si}} = 1 \times 10^{18} \text{ cm}^{-3}$ , above which carriers are able to transport via extended states and reasonable conductivities can be achieved. Therefore in order to obtain good n-type con-

Table 2. Electrical data of Si-doped  $\text{Al}_x\text{Ga}_{1-x}\text{N}$ -Improved results[after Ref. 14],  $N_{\text{Si}} = 5 \times 10^{18} \text{ cm}^{-3}$

$x$	0.5	0.6	0.65	0.7
	KSU-A597	KSU-A595	KSU-A594	KSU-A599
$\sigma(\Omega\text{-cm})^{-1}$	8.3	6.7	6.7	2.2
$\mu(\text{cm}^2/\text{Vs})$	33.6	30	20	21
$n(\text{cm}^{-3})$	$1.44 \times 10^{18}$	$1.9 \times 10^{18}$	$2.1 \times 10^{18}$	$6.2 \times 10^{17}$

ductivities in  $\text{Al}_x\text{Ga}_{1-x}\text{N}$  alloys ( $x \geq 0.4$ ), Si doping levels above  $1 \times 10^{18} \text{ cm}^{-3}$  is required. Indeed, by fixing the Si dopant concentration at  $5 \times 10^{18} \text{ cm}^{-3}$  while varying the growth conditions slightly, we have achieved highly conductive  $\text{Al}_x\text{Ga}_{1-x}\text{N}$  alloys with high Al contents ( $x$  up to 0.7). The Hall data for this new batch of samples are summarized in Table 2. Conductivity values of  $6.7 \Omega^{-1}\text{cm}^{-1}$  and  $2.2 \Omega^{-1}\text{cm}^{-1}$ , respectively, have been achieved for  $\text{Al}_{0.65}\text{Ga}_{0.35}\text{N}$  and  $\text{Al}_{0.7}\text{Ga}_{0.3}\text{N}$  alloys. We believe that the n-type conductivity values we have achieved here for  $\text{Al}_x\text{Ga}_{1-x}\text{N}$  alloys ( $x$  up to 0.7) are sufficiently high for deep UV ( $\sim 280 \text{ nm}$ ) emitter applications.

Because of our unique optical characterization capability, recently we have also successfully grown AlN epilayers on sapphire with high optical quality. For the first time, we have produced AlN epilayers that emit band-edge PL transition lines [20]. Moreover, it was shown

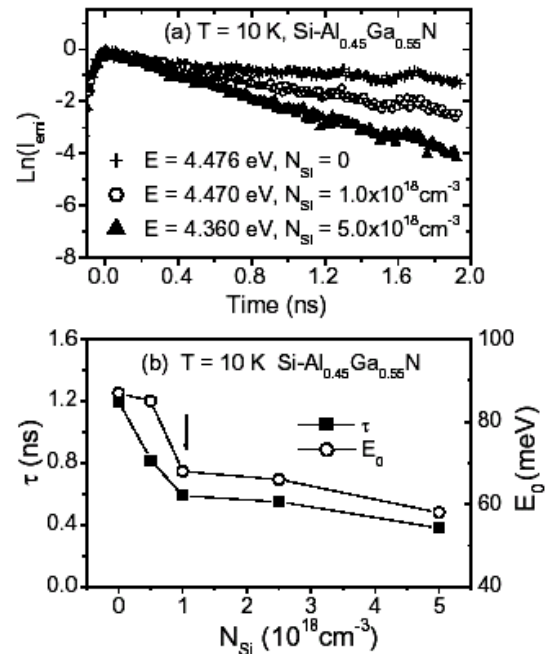


Fig. 4. (a) Time resolved PL emission spectra measured at 10 K for Si-doped  $\text{Al}_{0.45}\text{Ga}_{0.55}\text{N}$  alloys with three different Si doping concentrations. (b) The Si-doping concentration dependence of the measured decay time and activation energy  $E_0$  of Si-doped  $\text{Al}_x\text{Ga}_{1-x}\text{N}$  alloys [after Ref. 13].

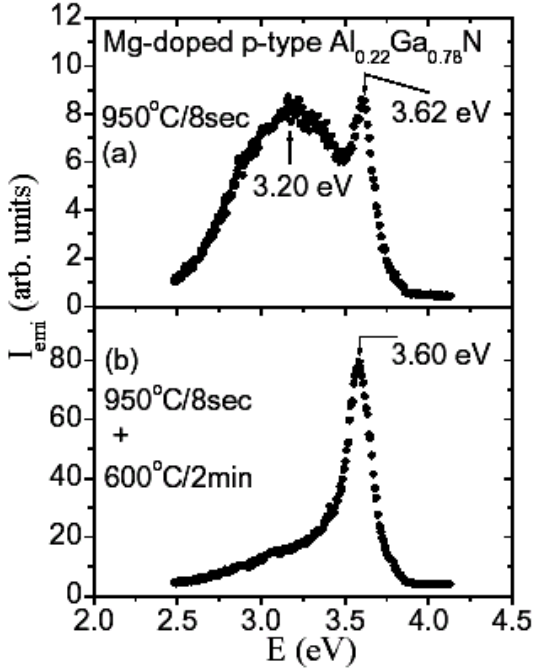


Fig. 5. Room temperature (300 K) cw-PL spectra of the Mg-doped p-type  $\text{Al}_{0.22}\text{Ga}_{0.78}\text{N}$  (a) after anneal of 950 °C for 8 s (b) after a second anneal at 600 °C for 2 min [after Ref. 14].

recently that the conductivity of AlN can indeed be controlled and n-type conduction with a free electron concentration of about  $1 \times 10^{17}\text{cm}^{-3}$  has been achieved by Si doping [21]. The demonstrated ability of achieving high optical quality as well as the n-type conductivity control of AlN further extends the applications of III-nitrides.

## 2. P-type AlGaN alloys

Figure 5(a) shows the room temperature (300 K) cw PL spectra of the Mg-doped p-type  $\text{Al}_x\text{Ga}_{1-x}\text{N}$  for  $x = 0.22$  after anneal of 950 °C for 8 sec and two emission peaks at 3.2 eV and 3.62 eV are observed. The emission peak at 3.2 eV is the main peak and in some of the samples studied, this was the only peak observed. The 3.2 eV transition has been well documented in Mg-doped p-type GaN, which is located at 2.95 eV [22]. A further anneal at 600 °C for 2 min in nitrogen gas resulted in the spectrum shown in Fig. 5 (b) where the peak at 3.2 eV is now reduced significantly at room temperature. The peak at 3.62 eV is slightly red-shifted to 3.60 eV but is now predominant, with about an order of increase in the emission intensity.

Fig. 6 shows room temperature (300 K) cw PL spectra of the Mg-doped p-type  $\text{Al}_x\text{Ga}_{1-x}\text{N}$  for  $x = 0.22$ , 0.25 and 0.27, following the two-step anneals described above. As can be seen, the emission intensities of these

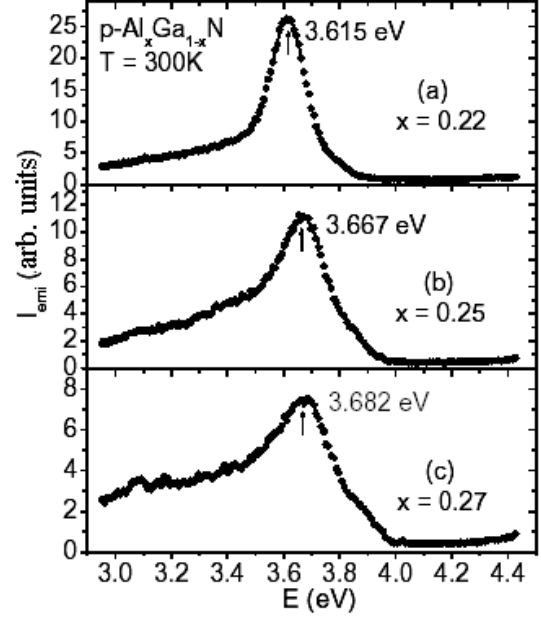


Fig. 6. . Room temperature (300 K) cw PL spectra from Mg-doped p-type  $\text{Al}_x\text{Ga}_{1-x}\text{N}$  for (a)  $x = 0.22$ , (b)  $x = 0.25$  and (c)  $x = 0.27$  [after Ref. 14].

spectra decrease with increase in  $x$ , a phenomenon we observed previously [23] which is related to reduction in crystalline quality with increasing  $x$ . The emission peaks are observed at 3.615 eV, 3.667 eV and 3.682 eV for  $x = 0.22$ , 0.25 and 0.27 respectively, which are greater than the band edge transition of 3.42 eV for GaN. We assign these emission lines to the band-to-impurity transitions for the recombination of free electrons with neutral Mg acceptors in  $\text{Al}_x\text{Ga}_{1-x}\text{N}$ . With the origin of these peaks thus assigned, the activation energy  $E_A(x)$  of the ionized Mg impurity in  $\text{Al}_x\text{Ga}_{1-x}\text{N}$  can be deduced simply by the difference between the energy gap  $E_g(x)$  and the observed band-to-impurity emission peak  $E(e^-, A^o)$ .  $E_g(x)$  can be estimated from the expression

$$E_g(x) = (1 - x)E_{g,\text{GaN}} + xE_{g,\text{AlN}} - bx(1 - x), \quad (2)$$

and  $E_A(x) = E_g(x) - E(e^-, A^o)$ . In the above expression, we used widely accepted value of the energy gap for GaN,  $E_{g,\text{GaN}} = 3.42$  eV, for AlN,  $E_{g,\text{AlN}} = 6.20$  eV and of the bowing parameter  $b = 0.90$  [24]. With these,  $E_A$  values of 0.262 eV, 0.279 eV and 0.311 eV corresponding to Al contents 0.22, 0.25 and 0.27, respectively, are obtained. It is expected that different choices of the bowing parameter  $b$  would result in variations in the  $E_A$  values. However, because the Mg acceptor level in AlGaN alloys is quite deep, the uncertainties in the  $E_A$  values due to different choices of  $b$  are not very significant. For example, the above optically obtained  $E_A$  values from Eq. (2) will be reduced by about 17 - 20 meV if the bowing parameter  $b = 1$  is used.

The values of  $E_A$  we obtained in the above manner are plotted as a function of Al content  $x$  in Fig. 7,

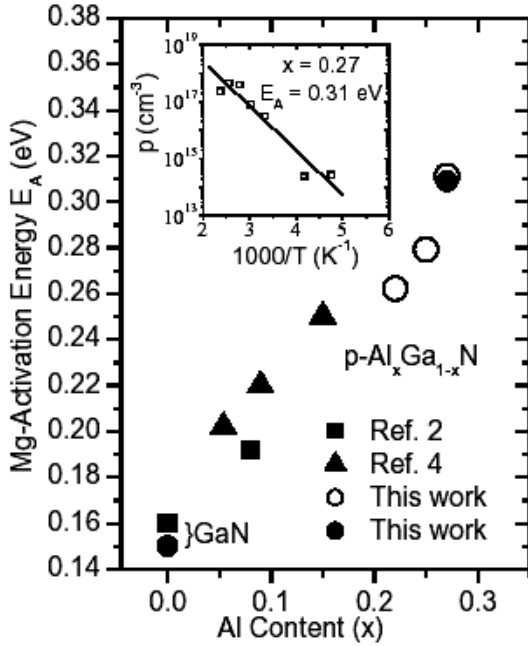


Fig. 7. Activation energies of Mg acceptors in Mg-doped p-type  $Al_xGa_{1-x}N$  as a function of Al content  $x$ . Closed squares and triangles are data from Ref. 9 and 11 respectively, while closed circles are data from our work, all obtained by Hall measurements. Open circles indicate data obtained by PL measurements from our work. The inset shows measured temperature dependence of Hall concentration ( $p$ ) in the Mg-doped p-type  $Al_{0.27}Ga_{0.73}N$  sample from which  $E_A = 0.310$  eV was obtained [after Ref. 14].

together with those reported previously [9,11], all obtained by means of variable temperature Hall measurements. Also shown in this figure are data points for p-GaN and for p- $Al_{0.27}Ga_{0.73}N$  where we determined  $E_A$  by variable temperature Hall measurements (0.15 eV and 0.309 eV respectively). The measured temperature dependence of Hall concentration ( $p$ ) in the Mg-doped p-type  $Al_{0.27}Ga_{0.73}N$  sample is shown in the inset of Fig. 7, from which a value  $E_A = 0.310$  eV was obtained. Since the hole concentrations in AlGaN alloys are relatively low and impurity band formation is not likely, our results of  $E_A$  deduced from the PL spectra match quite well with those obtained by Hall measurements, which further corroborates our assignment that the observed transitions between 3.62 - 3.68 eV in Fig. 6 are band-to-impurity transitions of free electrons to the neutral Mg acceptors. The increase of  $E_A$  with increase in band gap energy for the III-nitrides has been reported previously in other studies [9,11,25] and is predicted by the effective mass theory [26-28]. As a comparison with our results, the value of  $E_A$  estimated from the effective mass theory for  $x = 0.25$  for example, is between 0.263 and 0.294 eV which agrees with the measured value of 0.279 eV.

From the measured  $E_A$  versus  $x$  in Mg-doped p-type  $Al_xGa_{1-x}N$ , the resistivity versus  $x$  can be estimated as

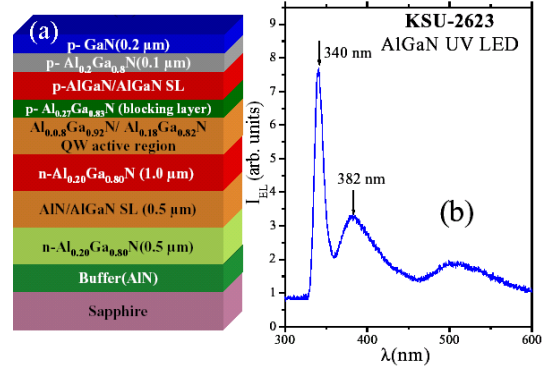


Fig. 8. Basic layer structure employed for 340 nm UV emitters in which p- $Al_xGa_{1-x}N$  ( $x \sim 0.27$ ) is employed as a blocking layer. (b) Electroluminescence (EL) spectrum of a 340 nm UV LED based on AlGaN QW.

follows:

$$\begin{aligned} \rho (Al_xGa_{1-x}N) &= \rho_0 \exp(E_A/kT) \\ &= \rho_0 \exp[E_A(GaN) + \Delta E_A]/kT \\ &= \rho_0(GaN) \exp(\Delta E_A/kT), \end{aligned} \quad (3)$$

where  $\Delta E_A = E_A(Al_xGa_{1-x}N) - E_A(GaN)$  and our typical p-type GaN has a resistivity of about  $1.0 \Omega\text{-cm}$ . From Eq. (3), the resistivity of  $Al_xGa_{1-x}N$  alloys with higher values of  $x$  can be deduced. For example, if the trend in Fig. 7 holds for higher  $x$ , at Al content  $x = 0.45$ , the activation energy  $E_A$  is estimated to be 0.4 eV and the estimated resistivity should be as high as  $2.2 \times 10^4 \Omega\text{-cm}$ . The fundamental property of Mg acceptors in AlGaN alloys (*i.e.*, Mg acceptor energy level deepening with increasing Al content) could be a “show-stop” for the achievement of high performance deep UV photonics devices based on III-nitrides. These results thus indicated that alternative methods for acceptor activation in AlGaN or InAlGaN alloys with high Al contents have to be developed.

By incorporating these p-type  $Al_{0.27}Ga_{0.73}N$  alloys into the emitter structures as the blocking layers, we have achieved the operation of 340 nm UV LEDs based on  $Al_{0.08}Ga_{0.92}N/Al_{0.18}Ga_{0.82}N$  QWs. Fig. 8 shows an electroluminescence spectrum of a 340 nm UV LED

#### IV. SUMMARY

As of this writing, rapid progress has been made recently in the area of III-nitride UV emitters. Recently, Professor Asif Khan’s group at University of South Carolina has achieved UV LEDs with emission wavelengths shorter than 340 nm and milliwatts output power under pulsed operation [29]. Most recently, Professor M. Razeghi’s group at Northwestern University has demonstrated the operation of a 280 nm UV LED under pulsed operation [30]. All these recent results demonstrate that

III-nitride materials are very promising for UV photonic device applications. However, there are many problems and questions that still stand in the way of the practical device implementation of deep UV emitters. Methods for improved material qualities as well as doping efficiencies still need to be further explored. Novel approaches for ohmic contact fabrication, p-type contacts in particular, must be further developed to curtail the problem of very low p-type conductivity in AlGa<sub>N</sub> alloys with high Al contents. A better understanding of fundamental properties of AlGa<sub>N</sub> alloys and their associated QWs with high Al contents is essential. For examples, the use of AlN bulk single crystals as substrates is expected to reduce crystal defect densities as well as UV photon absorption in UV emitter structures due to its better lattice constant and thermal expansion coefficient matches over other substrates, high thermal conductivity, and large energy gap. On the other hands, the incorporation of AlGa<sub>N</sub> or InAlGa<sub>N</sub> superlattice structures [31–33] and tunnel junctions p<sup>++</sup>/n<sup>++</sup> [34] are good examples of new approaches for tackling the problem of low p-type conductivities of AlGa<sub>N</sub>.

### ACKNOWLEDGMENTS

This research is supported by grants from DARPA, BMDO, ARO, ONR, DOE (96ER45604/A000), and NSF (DMR-9902431 and DMR-0203370). We would like to acknowledge the contributions of the following members of our group: J. Li, K. H. Kim, K. B. Nam, M. L. Nakarmi, J. Shakya, and T. N. Order.

### REFERENCES

- [1] J. R. Lakowicz, *Principle of Fluorescence Spectroscopy* 2nd edition (Kluwer Academic/Plenum Publisher, New York, 1999).
- [2] T. Tamamura, T. Setomoto and T. Taguchi, *J. Lumin.* **87**, 1180 (2000).
- [3] I. Akasaki and H. Amano, *Jpn. J. Appl. Phys.* **36**, 5393 (1997).
- [4] Y. Sato, N. Takahashi and S. Sato, *Jpn. J. Appl. Phys.* **35**, L838 (1996).
- [5] F. Hide, P. Kozodoy, S. P. Denbaars and A. J. Heeger, *Appl. Phys. Lett.* **70**, 2664 (1997).
- [6] M. A. Khan, V. Adivarahan, J. P. Zhang, C. Chen, E. Kuokstis, A. Chitnis, M. Shatalov, J. W. Yang and G. Simin, *Jpn. J. Appl. Phys.* **40**, L1308 (2001).
- [7] Nakamura and G. Fasol, *The Blue Laser Diode* (Springer, New York, 1997).
- [8] V. Adivarahan, G. Simin, G. Tamulaitis, R. Srinivasan, J. Yang and M. Asif Khan, *Appl. Phys. Lett.* **79**, 1903 (2001).
- [9] T. Tanaka, A. Watanabe, H. Amano, Y. Kobayashi, I. Akasaki, S. Yamazaki and M. Koike, *Appl. Phys. Lett.* **65**, 593 (1994).
- [10] I. Akasaki and H. Amano, *Mater. Res. Soc. Symp. Proc.* **242**, 383 (1991).
- [11] M. Suzuki, J. Nishio, M. Onomura and C. Hongo, *J. Cryst. Growth* **189/190**, 511 (1998).
- [12] L. Sugiura, M. Suzuki, J. Nishio, K. Itaya, Y. Kokubun and M. Ishikawa, *Jpn. J. Appl. Phys.* **7**, 3878 (1998).
- [13] K. B. Nam, J. Li, M. L. Nakarmi, J. Y. Lin and H. X. Jiang, *Appl. Phys. Lett.* **81**, 1038 (2002).
- [14] J. Li, T. N. Oder, M. L. Nakarmi, J. Y. Lin and H. X. Jiang, *Appl. Phys. Lett.* **80**, 1210 (2002).
- [15] <http://www.phys.ksu.edu/area/GaNgroup>.
- [16] Xiong Zhang, Soo-Jin Chua, Wei Liu and Kok-Boon Chong, *Appl. Phys. Lett.* **72**, 1890 (1998).
- [17] Z. Q. Li, H. Chen, H. F. Liu, L. Wan, M. H. Zhang, Q. Juang and J. M. Zhou, *Appl. Phys. Lett.* **76**, 3765 (2000).
- [18] S. Ruvimov, Z. Liliental-Weber, T. Suski, J. W. Ager III and J. Washburn, *Appl. Phys. Lett.* **69**, 990 (1996).
- [19] K. C. Zeng, J. Y. Lin, H. X. Jiang, A. Salvador, G. Popovici, H. Tang, W. Kim and H. Morkoc, *Appl. Phys. Lett.* **71**, 1368 (1997).
- [20] J. Li, K. B. Nam, M. L. Nakarmi, J. Y. Lin and H. X. Jiang, *Appl. Phys. Lett.* submitted.
- [21] Y. Taniyasu, M. Kasu and N. Kobayashi, *Appl. Phys. Lett.* **81**, 1255 (2002).
- [22] M. Smith, G. D. Chen, J. Y. Lin, H. X. Jiang, A. Salvador, B. N. Sverdlov, A. Botchkarev, H. Morkoc and B. Goldenberg, *Appl. Phys. Lett.* **68**, 1883 (1996).
- [23] H. S. Kim, R. A. Mair, J. Li, J. Y. Lin and H. X. Jiang, *Appl. Phys. Lett.* **76**, 1252 (2000).
- [24] Y. Koide, H. Itoh, M. R. H. Khan, K. Hiramato, N. Sawaki and I. Akasaki, *J. Appl. Phys.* **61**, 4540 (1987).
- [25] K. Kumakura, T. Makimoto and N. Kobayashi, *Jpn. J. Appl. Phys.* **39**, L337 (2000).
- [26] I. Akasaki and H. Amano, *Jpn. J. Appl. Phys.* **36**, 5393 (1997).
- [27] J. B. Xia, K. W. Cheah, X. L. Wang, D. Z. Sun and M. Y. Kong, *Phys. Rev. B* **59**, 10119 (1999).
- [28] F. Mireles and S. E. Ulloa, *Phys. Rev. B* **58**, 3879 (1998).
- [29] M. Asif Khan, V. Adivarahan, J. P. Zhang, C. Chen, E. Kuokstis, A. Chitnis, M. Shatalov, J. W. Yang and G. Simin, *Jpn. J. Appl. Phys.* **40**, L1308 (2001).
- [30] A. Yasan, R. McClintock, K. Mayes, S. R. Darvish, P. Kung and M. Razeghi, *Appl. Phys. Lett.* **81**, 801 (2002).
- [31] P. Kozodoy, M. Hansen, S. P. DenBaars and U. K. Mishra, *Appl. Phys. Lett.* **74**, 3681 (1999).
- [32] P. Kozodoy, Y. P. Smorchkova, M. Hansen, H. Xing, S. P. DenBaars and U. K. Mishra, A. W. Saxler, P. Perrin, and W. C. Mitchel, *Appl. Phys. Lett.* **75**, 2444 (1999).
- [33] H. X. Jiang, S. X. Jin, J. Li, J. Shakya and J. Y. Lin, *Appl. Phys. Lett.* **78**, 1303 (2001).
- [34] S. R. Jeon, Y. H. Song, H. J. Jang, G. M. Yang, S. W. Hwang and S. J. Son, *Appl. Phys. Lett.* **78**, 3265 (2001).